Electronic Supplementary Information (ESI)

A novel fluorescent chemosensor enables dual-channel selective "turn-on" detection of Hg^{2+} and Ag^{+} via distinct thiophilic effects, essential mechanisms, and excellent sensing performance for mercury(II) in aggregated states

Zhijun Ruan*, Xinyi Dong, Tao Long*, Shanshan Liu, Yanmei Chen, Junqi Lin*

Hubei Key Laboratory of Processing and Application of Catalytic Materials, College of Chemistry and Chemical Engineering, Huanggang Normal University, Huanggang 438000, China

Experimental section

1. Material

Dichloromethane (DCM) and tetrahydrofuran (THF) was dried over and distilled from CaH_2. Triphenylamine (TPA), terephthaloyl dichloride, 1, 2-ethanedithiol, aluminum chloride ($AlCl_3$) and all the other reagents were purchased from commercial suppliers and directly used without further purification. Various inorganic salt: $Hg(ClO_4)_2·3H_2O$, $AgNO_3$, $LiNO_3$, $NaNO_3$, KNO_3, $Co(NO_3)_2·6H_2O$, $Cu(NO_3)_2·3H_2O$, $Pb(NO_3)_2$, $Cd(NO_3)_2·4H_2O$, $Ba(NO_3)_2$, $Ca(NO_3)_2·4H_2O$, $Mg(ClO_4)_2$, $Fe(ClO_4)_2$, $Zn(NO_3)_2·6H_2O$, $Mn(NO_3)_2·4H_2O$, $Ni(NO_3)_2·6H_2O$, $Al(NO_3)_3·9H_2O$, $Fe(NO_3)_3·9H_2O$ and $Cr(NO_3)_3·9H_2O$ was dissolved in ultra-pure water to afford $1×10^{-1}$ mol/L aqueous solution, respectively.

2. Instrumentation

^1H and ^{13}C NMR spectroscopy were recorded in $CDCl_3$ or THF-d_8 with a Varian Mercury 300 or Bruker ARX400 spectrometer using Me_4Si (TMS; δ = 0 ppm) as internal standard. Fourier transform infrared (FTIR) spectra were recorded on a Nicolet NEXUS-6700 FTIR spectrophotometer in the region of 400–4000 cm^{-1}. EI-MS spectrum was performed with a Finnigan PRACE mass spectrometer. Elemental analysis (EA) was conducted by a CARLOERBA-1106 micro-elemental analyzer. UV-Vis spectra were collected by using a Shimadzu UV-2600 spectrometer. Photoluminescence spectra were conducted on a Hitachi F-4700 spectrophotometer. The quantum yield was gained by a reference method with 9,10-Diphenylanthracene (λ_{ex} = 366 nm, Φ_F = 0.95) as the standard compound. Density functional theory (DFT) calculations were carried out based on the B3LYP/6-31G(d) basis set. Single crystals of **DTPAO** (CCDC 1876442) and **DTPAS** (CCDC 2267083) were obtained from DCM/n-hexane mixture and were then tested by X-ray crystallography.

The crystal analysis was performed over a Bruker SMART APEX II CCD diffractometer with graphite-monochromatized MoK_α radiation ($\lambda = 0.71073$ Å).

3. Fluorescence emission changes with different metal ions

To optimize the sensing performance of the probe, the effect of probe concentration of 10, 20 and 100 μM was investigated. Taking the detection of Ag^+ as an example, the employ of 20 μM **DTPAS** gave the highest linearity ($R^2 = 0.996$), the maximum linear ranges (0 to 50 μM) and the best fluorescence enhancement efficiency (41.2-fold) compared to the other two concentrations. Therefore, 20 μM was selected as the optimal concentration of probe.

Testing in pure solution: a solution of **DTPAS** (2×10^{-5} mol/L) in THF was prepared, then various metal ions (1×10^{-1} M, 18 μL) were added to the solution of **DTPAS** respectively. The resultant solutions (3 mL) were placed in a quartz cell (10.0 mm width) at room temperature, and the changes of the PL intensity were recorded each time (excitation wavelength 380 nm). Testing in aggregated state: different metal ions (1×10^{-1} M, 18 μL) were added to the solution of 60 μL **DTPAS** (1×10^{-3} M in THF) respectively, then distilled water was added to generate aggregated nanoparticles (with f_w = 98%). The changes of the PL spectra were recorded each time at room temperature (excitation wavelength 380 nm).

4. UV-Vis absorption spectra changes with different metal ions

Solution of **DTPAS** (2×10^{-5} mol/L) in THF was prepared, then various metal ions (1×10^{-1} M, 18 μL) were added to the solution of **DTPAS** respectively. The resultant solutions (3 mL) were placed in a quartz cell (10.0 mm width) at room temperature, and the changes of the UV-Vis absorption spectra were recorded each time.

5. Synthesis and characterization

*5.1 Synthesis of 1,4-phenylenebis((4-(diphenylamino)phenyl)methanone) (**DTPAO**)*

Triphenylamine (2.45 g, 10 mmol) and fully ground powder of anhydrous aluminum chloride ($AlCl_3$) (1.33 g, 10 mmol) were dissolved in 40 mL dry DCM, then terephthaloyl dichloride (1.02 g, 5 mmol) was added to the resultant suspension under stirring. After stirring for 24 h at 60 ℃, the reaction mixture was washed with saturated brine and extracted three times with DCM (3 × 60 mL), and dried over anhydrous Na_2SO_4. Then the organic solvent was evaporated under vacuum, and the residue was purified by column chromatography over silica gel using CH_2Cl_2–petroleum ether (6:1, v/v) mixture as eluent to afford a light yellow solid (1.92 g, 62%, m.p. 139–141 ℃). FTIR (thin film), *v* (cm^{-1}): 3036, 2923, 1649, 1584, 1554, 1489, 1311, 1274, 1153, 926, 865, 751, 695. ^{1}H NMR (300 MHz, $CDCl_3$): 7.82 (s, 4H, ArH), 7.73 (d, J = 9.0, 4H, ArH), 7.36 (m, 8H, ArH), 7.20 (m, 12H, ArH), 7.02 (d, J = 6.0, 4H, ArH). ^{13}C NMR (75 MHz, $CDCl_3$): 194.5, 152.3, 146.3, 141.1, 132.1, 129.7, 129.3, 128.9, 126.2, 124.9, 119.3. MS (EI): calcd for 620.2; found: 620.5. Anal. calcd for $C_{44}H_{32}N_2O_2$: C 85.14, H 5.20, N 4.51; found: C 84. 89, H 5.02, N 4.48.

*5.2 Synthesis of (4-(diphenylamino)phenyl)(4-(2-(4-(diphenylamino)phenyl)-1,3-dithiolan-2-yl) phenyl)methanone (**DTPAOS**)*

Compound **DTPAO** (0.62 g, 1 mmol) and 1, 2-ethanedithiol (0.17 mL, 2 mmol) were dissolved in 15 mL dry DCM, then BF_3 Ɛt_2O (0.50 mL, 4 mmol) as the Lewis acid was added. After stirring overnight at room temperature, aqueous $NaHCO_3$ was added to the reaction mixture to adjust the pH value of 8–9. The resultant solution was extracted with DCM for three times (3 × 40 mL) and dried over anhydrous Na_2SO_4. Then the organic solvent was evaporated under vacuum, and the residue was purified by column chromatography over silica gel using CH_2Cl_2–petroleum ether (2:1, v/v) mixture as eluent to afford a light yellow solid (0.49 g, 70%, m.p. 119–121 ℃). FTIR (thin film), *v*

(cm^{-1}): 2955, 2924, 2853, 1646, 1583, 1488, 1310, 1273, 1176, 930, 753, 695. ^{1}H NMR (300 MHz, $CDCl_3$): 7.76 (m, 6H, ArH), 7.40 (m, 6H, ArH), 7.25 (m, 14H, ArH), 7.08 (m, 6H, ArH), 3.53 (m, 4H, -SCH_2-). ^{13}C NMR (75 MHz, $CDCl_3$): 194.7, 152.0, 148.9, 147.4, 147.0, 146.5, 136.8, 132.0, 129.7, 129.4, 129.3, 129.0, 128.1, 126.0, 124.7, 123.2, 122.2, 119.3, 76.4, 40.3. MS (EI): calcd for 696.2; found: 695.8. Anal. calcd for $C_{46}H_{36}N_2OS_2$: C 79.28, H 5.21, N 4.02; found: C 78.95, H 5.39, N 4.11.

*5.3 Synthesis of 4,4'-(2,2'-(1,4-phenylene)bis(1,3-dithiolane-2,2-diyl))bis(N,N-diphenylaniline) (**DTPAS**)*

DTPAS was prepared via the same procedure to that of **DTPAOS** with adjusted feed ratio, 1 mmol **DTPAO**, 4 mmol 1, 2-ethanedithiol and 8 mmol BF_3·Et_2O. The crude product was purified by column chromatography over silica gel using CH_2Cl_2–petroleum ether (1:1, v/v) mixture as eluent to afford a pale solid (0.35 g, 36%, m.p. 243–245 ℃). FTIR (thin film), *v* (cm^{-1}): 3032, 2922, 2850, 1589, 1493, 1313, 1274, 1179, 1018, 753, 695. ^{1}H NMR (300 MHz, THF-d_8): 7.54 (s, 4H, ArH), 7.44 (d, J = 9.0, 4H, ArH), 7.22 (t, J = 6.0, 8H, ArH), 7.06 (d, J = 6.0, 8H, ArH), 7.00 (t, J = 6.0, 4H, ArH), 6.91 (d, J = 6.0, 4H, ArH), 7.02 (d, J = 6.0, 4H, ArH), 3.58 (m, 8H, -SCH_2-). ^{13}C NMR (75 MHz, THF-d_8): 147.7, 146.8, 143.7, 137.8, 129.3, 129.1, 127.8, 124.4, 122.9, 121.9, 76.4, 39.9. MS (EI): calcd for 772.2; found: 772.6. Anal. calcd for $C_{48}H_{40}N_2S_4$: C 74.57, H 5.22, N 3.62; found: C 74.28, H 5.33, N 3.47.

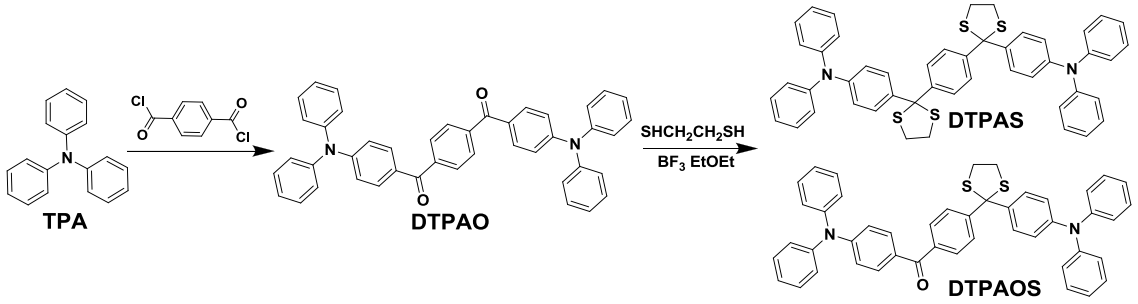

Scheme S1. Synthetic pathway of **DTPAS** and **DTPAOS**.

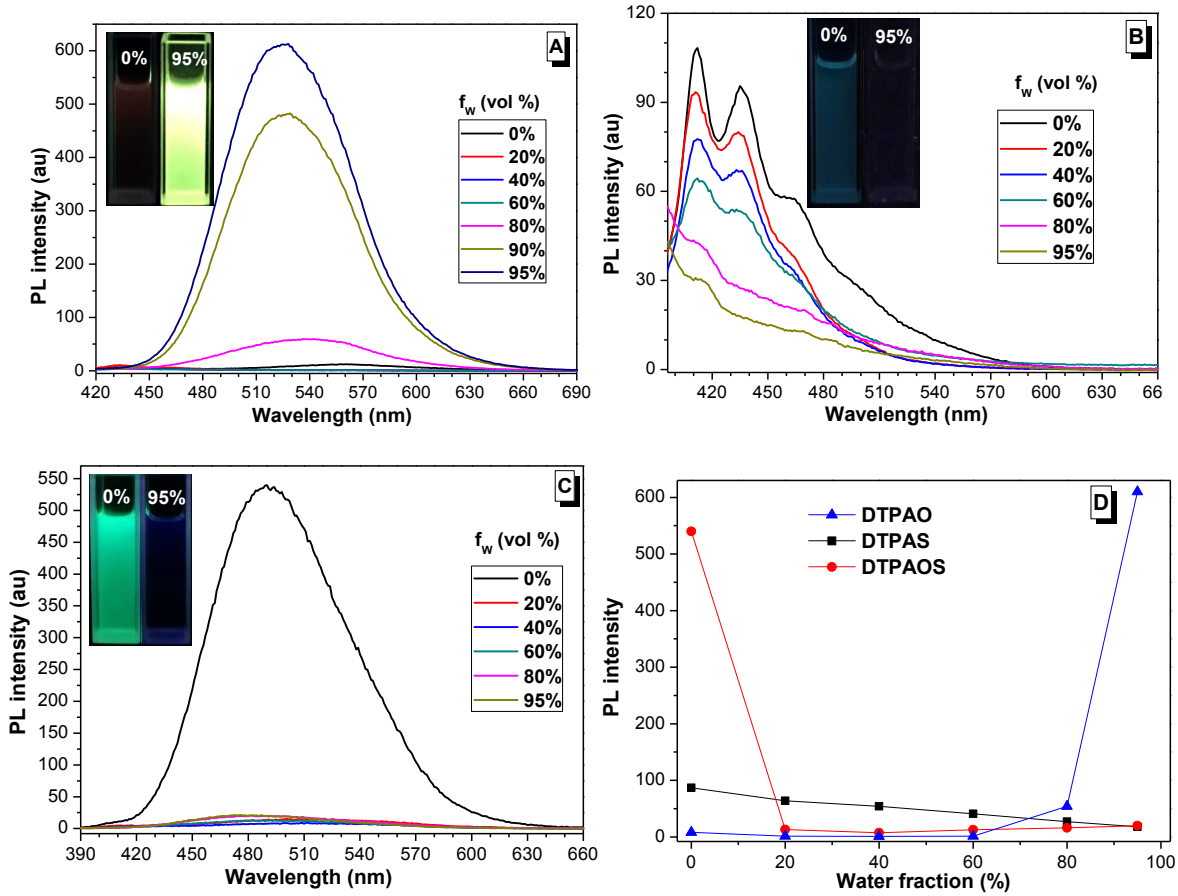

Fig. S1 PL spectra of **DTPAO** (a), **DTPAS** (b) and **DTPAOS** (c) in THF/H_2O mixtures (20 μM) with different water fractions. Inset: Photos of luminogens in THF/H_2O mixtures taken under the illumination of a 365 nm UV lamp. (d) Changes of PL peak intensity with water fractions.

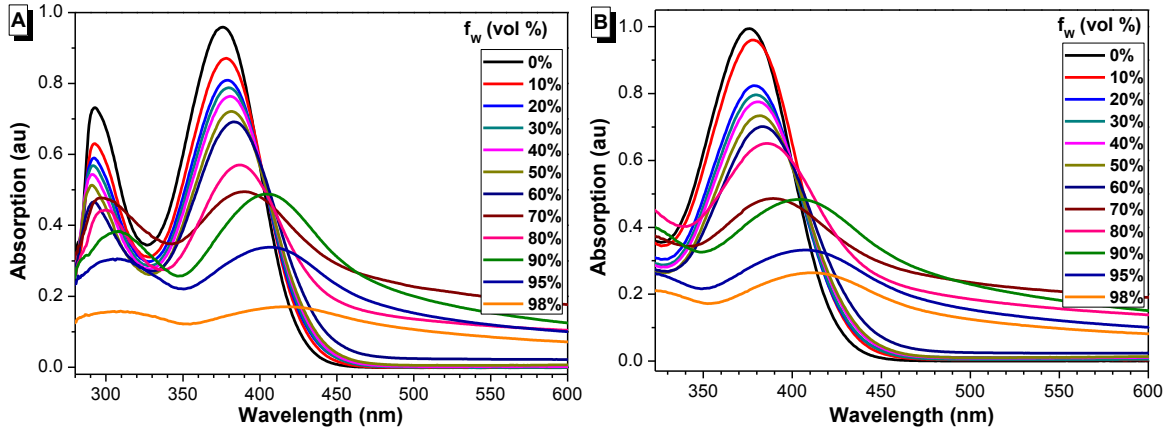

Fig. S2 UV-Vis spectra of **DTPAO** (a) and **DTPAS**+Hg^{2+} (b) in THF/H_2O mixtures with different water fractions.

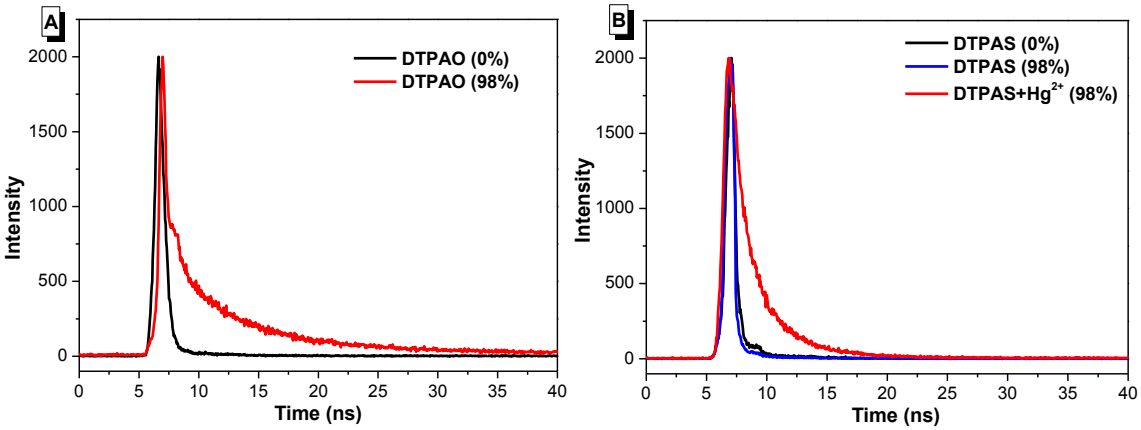

Fig. S3 Time-resolved photoluminescence spectra of **DTPAO** (a), **DTPAS** and **DTPAS**+Hg^{2+} (b) with water fractions as 0% and 98%.

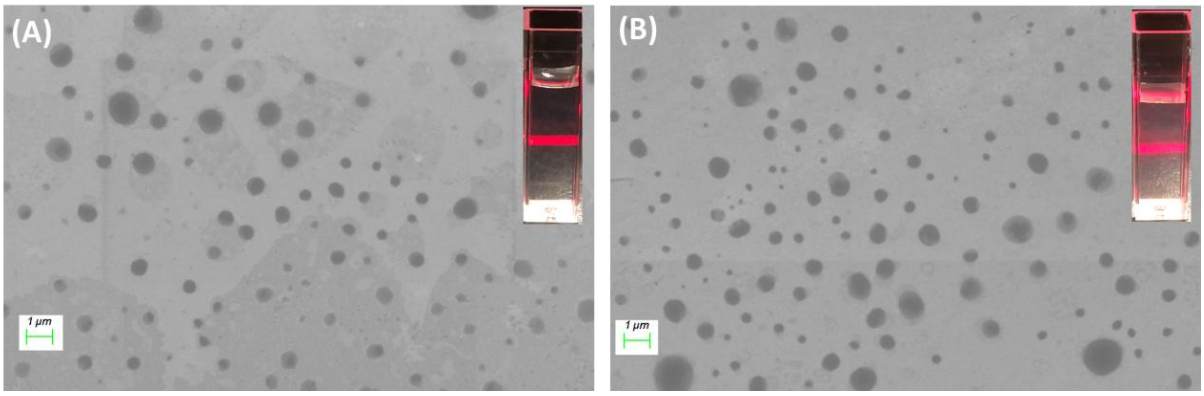

Fig. S4 Scanning electron microscopy and image of the Tyndall effect of **DTPAO** (a), **DTPAS**+Hg^{2+} (b) with water fractions as 98%.

Table S1 Photophysical data of **DTPAO**, **DTPAOS** and **DTPAS**.

Sample	λ_{max}, (nm)[a]	PL λ_{em} (nm)	Φ_F (%)[a]	Φ_F (%)[b]	Φ_F (%)[c]	Lifetime (ns)[a]	Lifetime (ns)[b]
DTPAO	292, 376	562[a], 525[b]	3.6	36.4	38.2	5.4	10.5
DTPAOS	296, 364	491[a]	45.2	0.6	1.3	12.6	3.9
DTPAS	307	412, 435[a]	0.9	0.2	0.3	4.3	2.2

[a] Photophysical data determined in THF (20 μM); [b] determined in THF-water mixtures (f_w = 98%, 20 μM); [c] determined in solid state.

Table S2 Summary of crystal data and intensity collection parameters for **DTPAO** and **DTPAS**.

Compound	**DTPAO**	**DTPAS**
Formula	$C_{44}H_{32}N_2O_2 \cdot 1/2(C_6H_{14})$	$C_{48}H_{40}N_2S_4$
Formula mass	663.80	773.06
Wavelength/Å	0.71073	1.54178
Temperature/K	273(2)	296(2)
Space group	Triclinic, P-1	Monoclinic, C2/c
a/Å	10.429(4)	45.1405(16)
b/Å	11.065(4)	7.6554(3)
c/Å	15.589(5)	11.8691(5)
α/°	93.724(6)	90.00
β/°	102.674(6)	104.164(4)
γ/°	90.425(6)	90.00
V / Å^3	1750.9(10)	3976.9(3)
Z/mg.m^{-3}	2, 1.259	4, 1.291
F000	702	1624
Theta range/°	1.342 to 24.820	2.019 to 68.336
No. of collected reflns	12103	12926
No. of unique reflns.	5932	3469
Rint	0.0439	0.0594
Data/restrains/parameters	5932/0/461	3469/0/244
R1,wR2[obs I>2σ(I)]	R1 = 0.0633, wR2 = 0.1832	R1 = 0.0438, wR2 = 0.1137
R1,wR2 (all data)	R1 = 0.0962, wR2 = 0.2235	R1 = 0.0645, wR2 = 0.1253
Residual peak/hole e. Å^{-3}	0.866 and -0.277	0.164 and -0.229
CCDC number	1876442	2267083

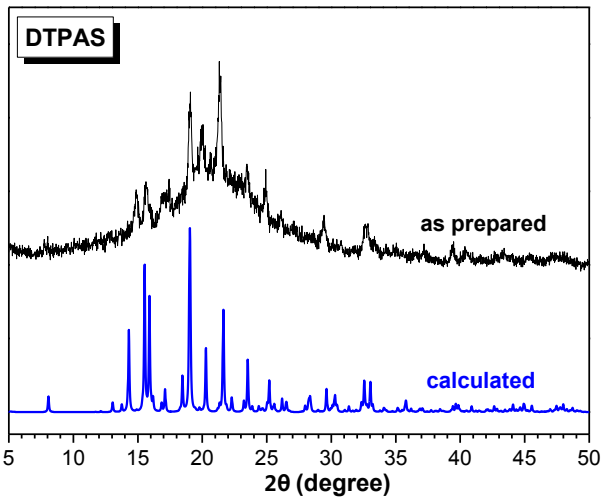

Fig. S5 XRD of the as-prepared solid of **DTPAS** and its calculated PXRD pattern.

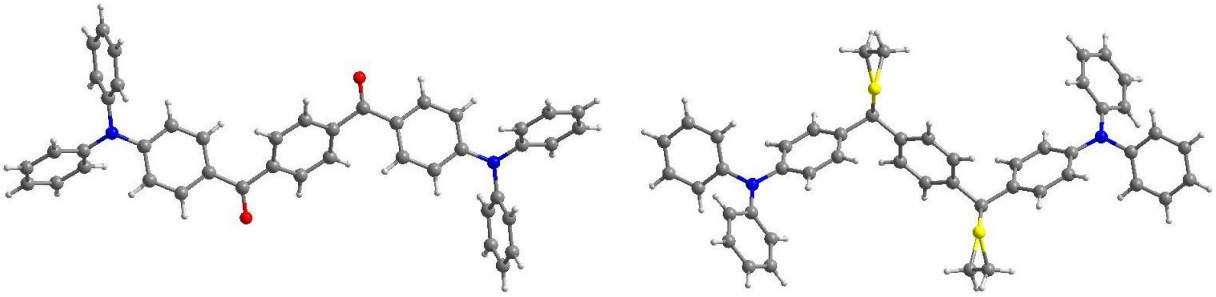

Fig. S6 Molecular structures of **DTPAO** and **DTPAS** in the single crystal.

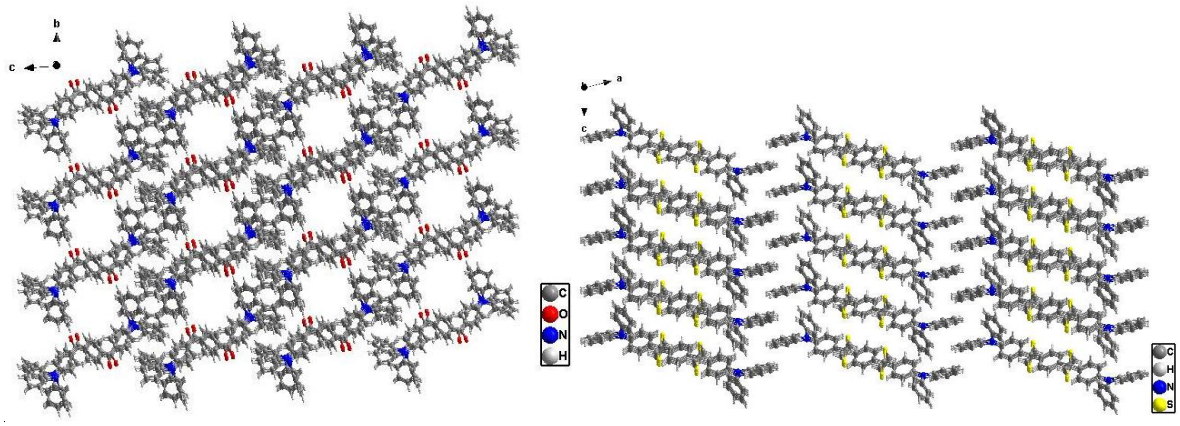

Fig. S7 Molecular packing mode of **DTPAO** and **DTPAS** crystals.

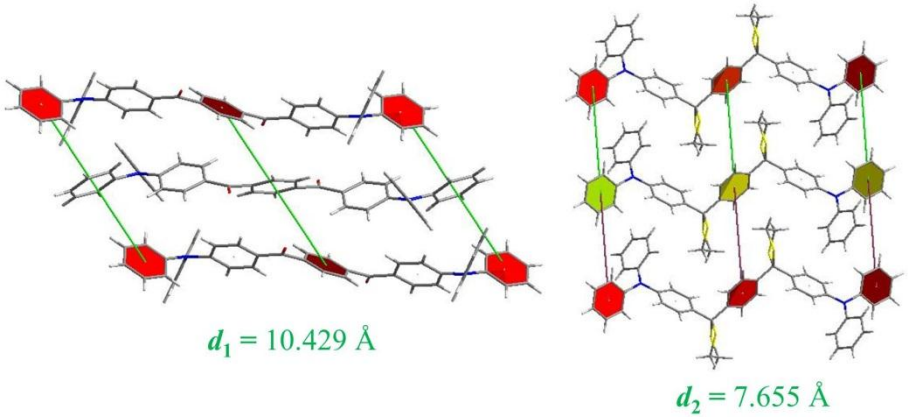

Fig. S8 The π–π distances for **DTPAO** (left) and **DTPAS** (right).

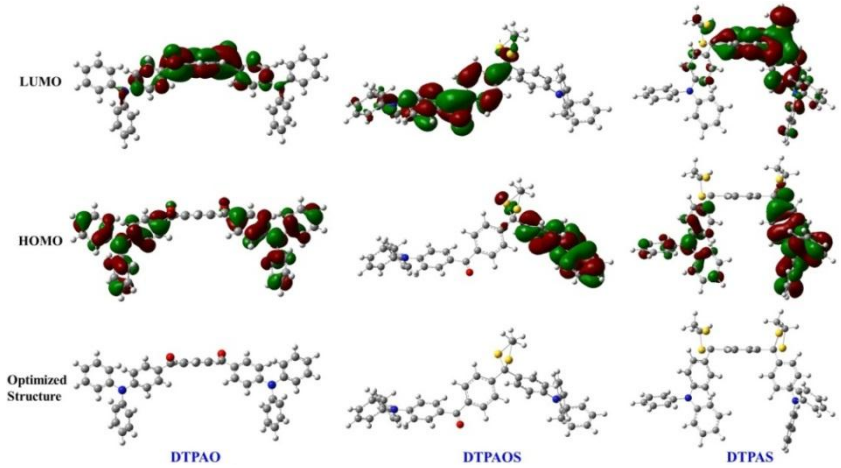

Fig. S9 Calculated molecular orbital amplitude plots of HOMO and LUMO levels and optimized molecular structures of **DTPAO**, **DTPAOS** and **DTPAS**.

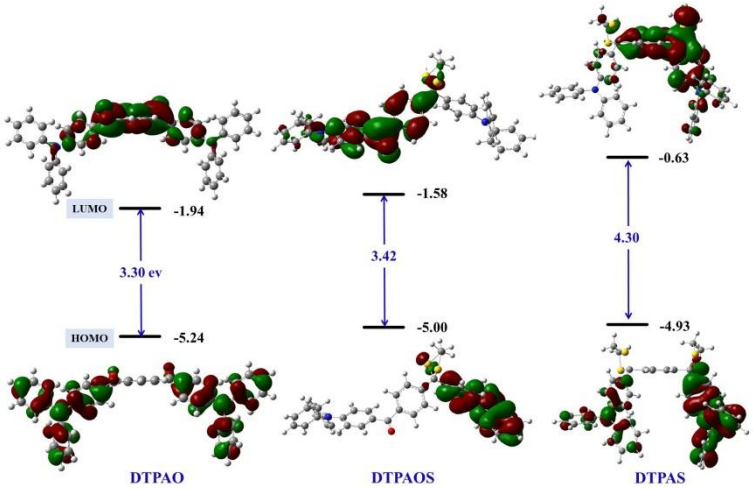

Fig. S10 HOMO, LUMO and corresponding energy gaps of **DTPAO**, **DTPAOS** and **DTPAS** based on optimized molecular structures.

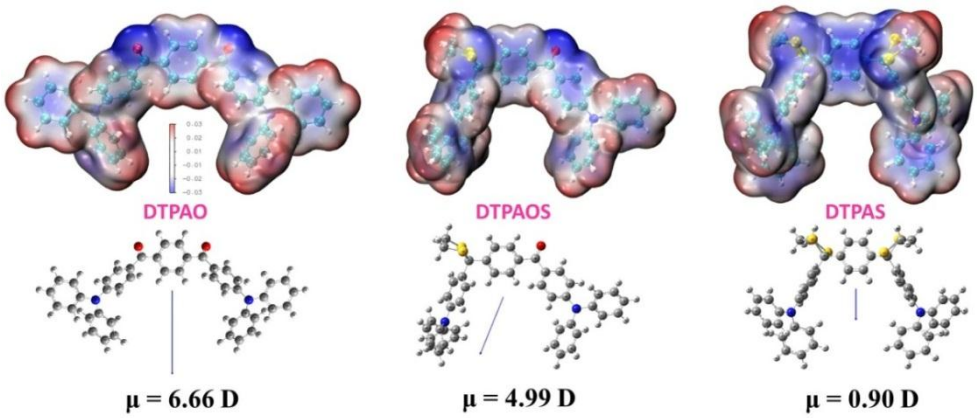

Fig. S11 ESP maps and the dipole moment of **DTPAO**, **DTPAOS** and **DTPAS**.

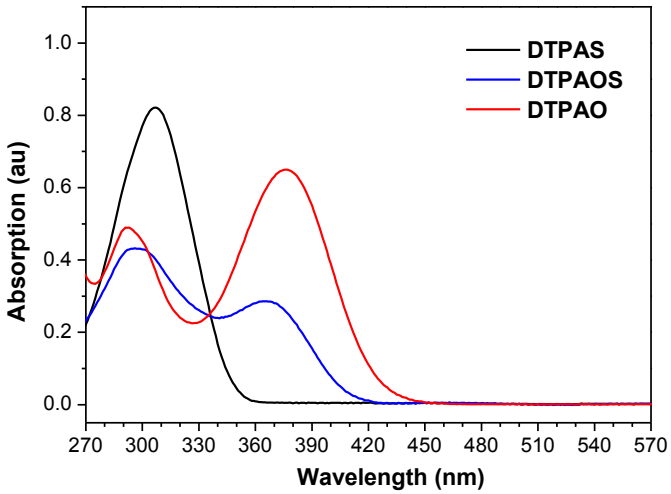

Fig. S12 UV-Vis spectra of **DTPAO**, **DTPAOS** and **DTPAS** in THF.

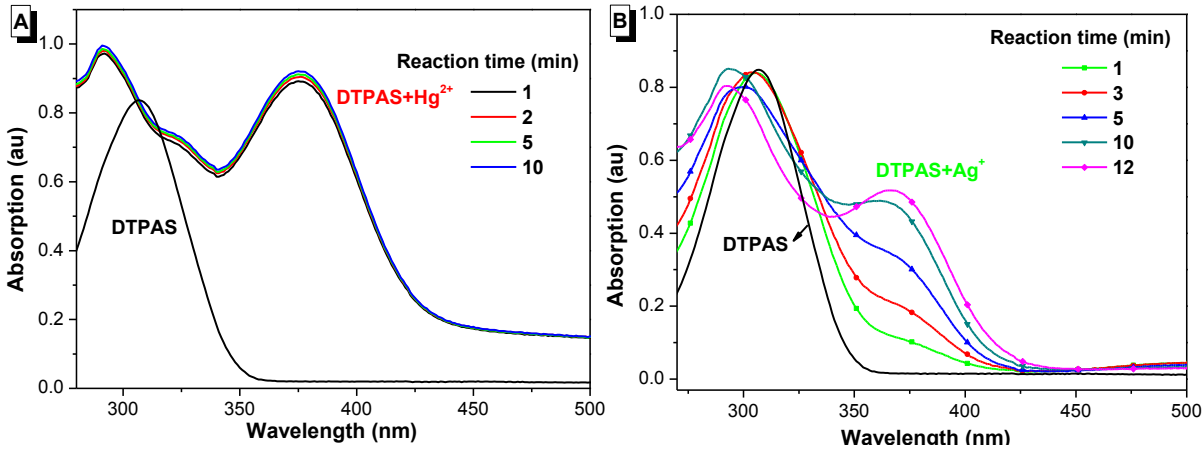

Fig. S13 UV-Vis absorption spectra of **DTPAS** in presence of Hg^{2+} (a) and Ag^{+} (b) under different reaction time in THF.

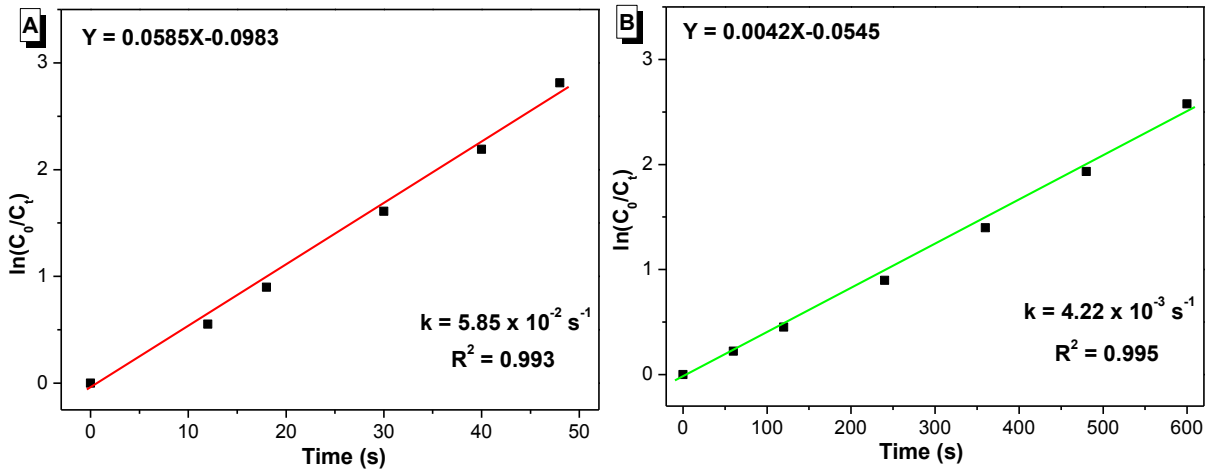

Fig. S14 Pseudo-first-order kinetics plots for **DTPAS** reacted with Hg^{2+} (a) and Ag^{+} (b), respectively. C_0 is the $[\mathbf{DTPAS}]_0$ at time t = 0 and C_t is the $[\mathbf{DTPAS}]_t$ at time t. The rate constant (k) is calculated as $\ln C_0/C_t = kt$.

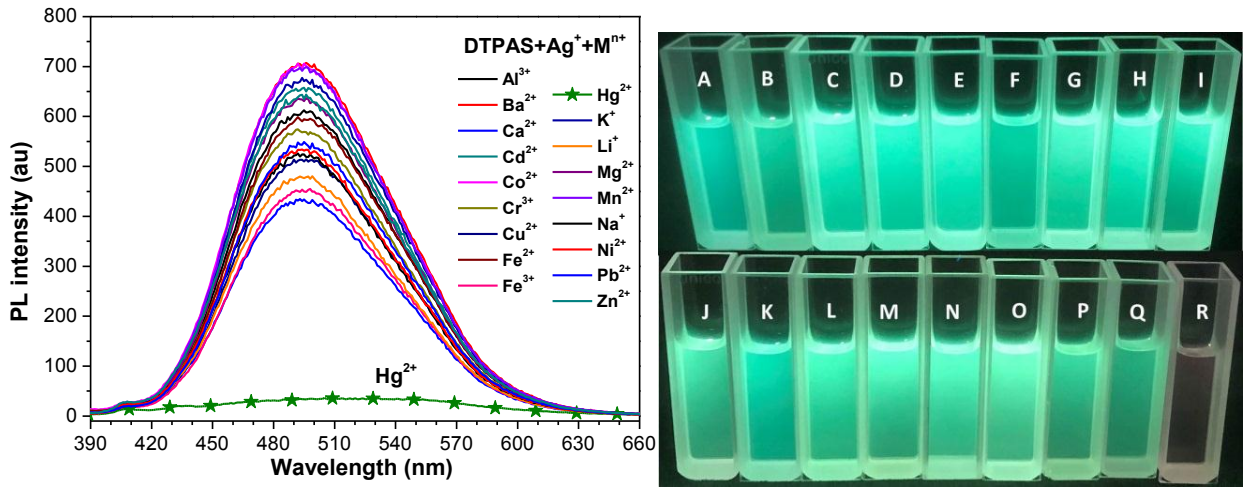

Fig. S15 PL spectra and fluorescence photos of **DTPAS** (20 μM) reacted with Ag^{+} in the presence of various metal ions (6 $\times 10^{-4}$ M) in THF solution. (A-R) **DTPAS+Ag^{+}**+ Al^{3+}, Fe^{3+}, Cu^{2+}, Pb^{2+}, Co^{2+}, Cr^{3+}, Cd^{2+}, Mg^{2+}, Mn^{2+}, Ba^{2+}, Fe^{2+}, Ca^{2+}, Ni^{2+}, Zn^{2+}, Li^{+}, K^{+}, Na^{+}, Hg^{2+}.

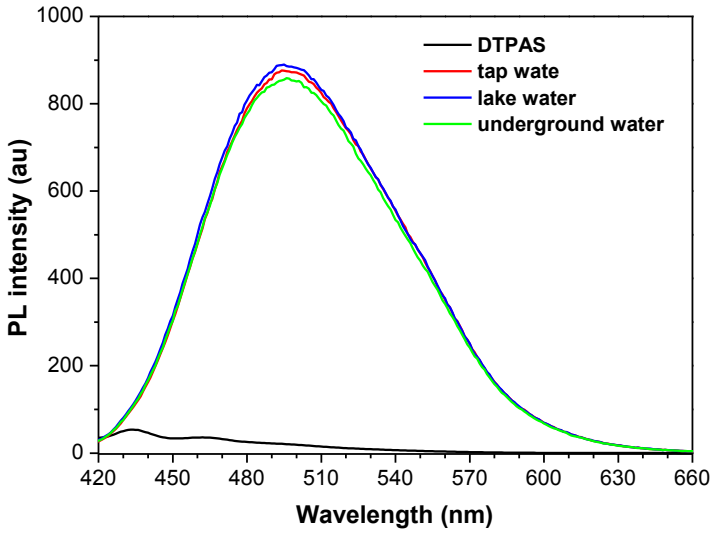

Fig. S16 PL spectra of **DTPAS** (10 μM) in THF, and **DTPAS** reacted with Ag^{+} (3 $\times 10^{-4}$ M) in tap water, lake water and underground water.

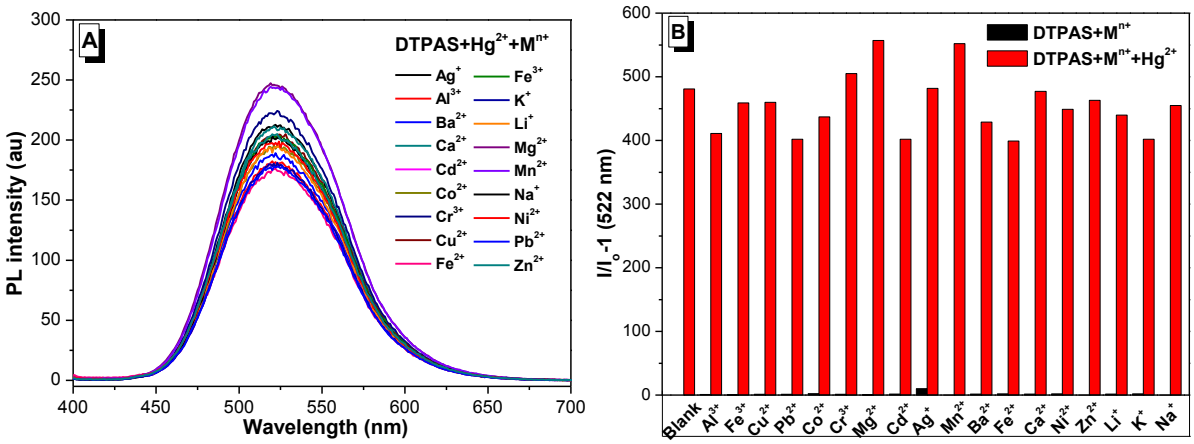

Fig. S17 (a) PL spectra of **DTPAS** (20 μM) in the presence of Hg^{2+} and various metal ions (6 $\times 10^{-4}$ M) in THF-H_2O mixtures with f_W = 98%.(b) Fluorescence spectra profiles of **DTPAS** (20 μM) in the presence of various metal ions and Hg^{2+} (6 $\times 10^{-4}$ M, red line) in THF-H_2O mixtures with f_W = 98%.

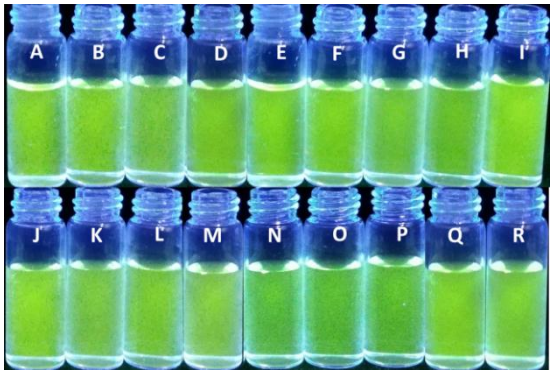

Fig. S18 Fluorescence photos of **DTPAS** (20 μM) reacted with Hg^{2+} in the presence of various metal ions (6 $\times 10^{-4}$ M) in THF/H_2O (2/98, v/v) solution. (A-R) **DTPAS+Hg^{2+}**+Ag^{+}, Al^{3+}, Fe^{3+}, Cu^{2+}, Pb^{2+}, Co^{2+}, Cr^{3+}, Cd^{2+}, Mg^{2+}, Mn^{2+}, Ba^{2+}, Fe^{2+}, Ca^{2+}, Ni^{2+}, Zn^{2+}, Li^{+}, K^{+}, Na^{+}.

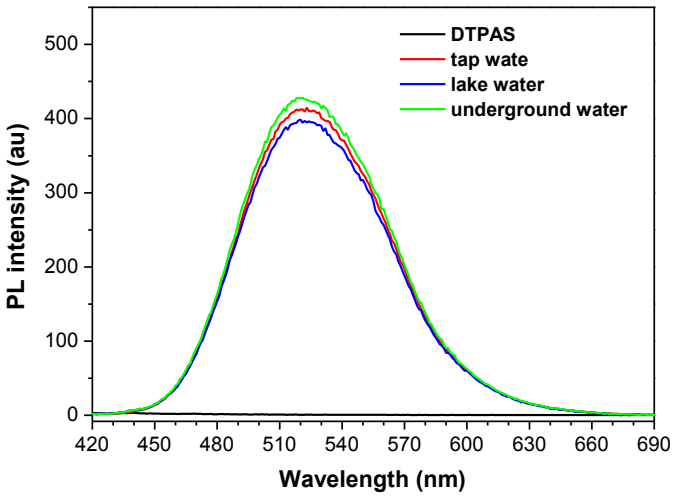

Fig. S19 PL spectra of **DTPAS** (10 μM) and **DTPAS** reacted with Hg^{2+} (3×10^{-4} M) in tap water, lake water and underground water in THF/H_2O with f_W = 98%.

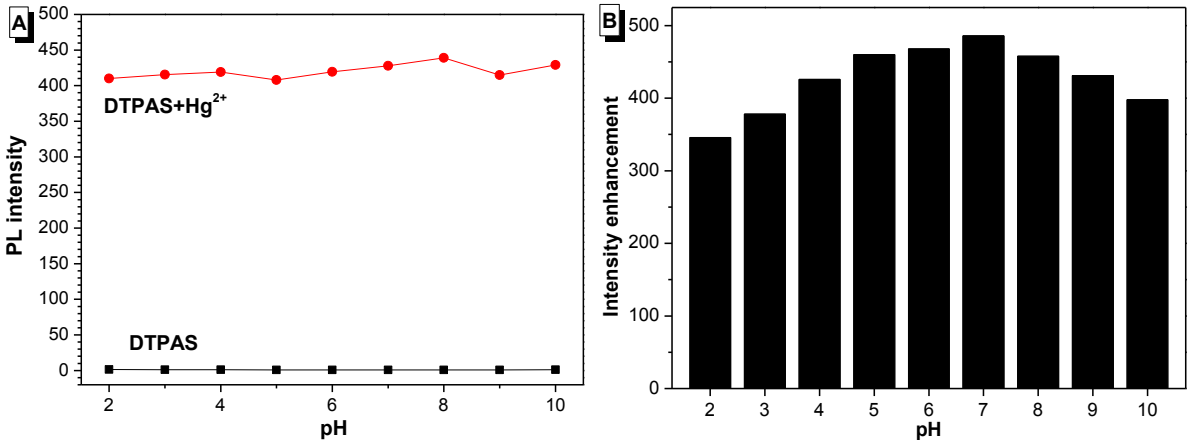

Fig. S20 (a) PL intensity of **DTPAS** and **DTPAS+Hg^{2+}** at different pH values with f_W = 98%. (b) PL intensity enhancement of **DTPAS** (20 μM) in the presence of Hg^{2+} (6×10^{-4} M) at different pH values.

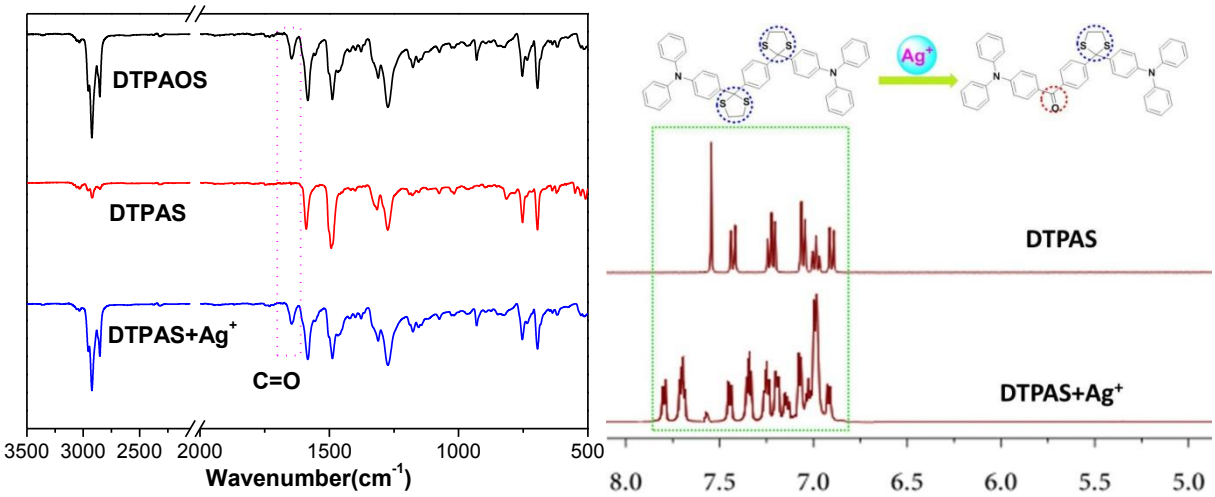

Fig. S21 IR spectra of **DTPAOS**, **DTPAS** and the reaction product of **DTPAS+Ag**$^{+}$ (left). ^{1}H NMR spectra of **DTPAS** (THF-*d8*) before and after the addition of Ag^{+} ions (right).

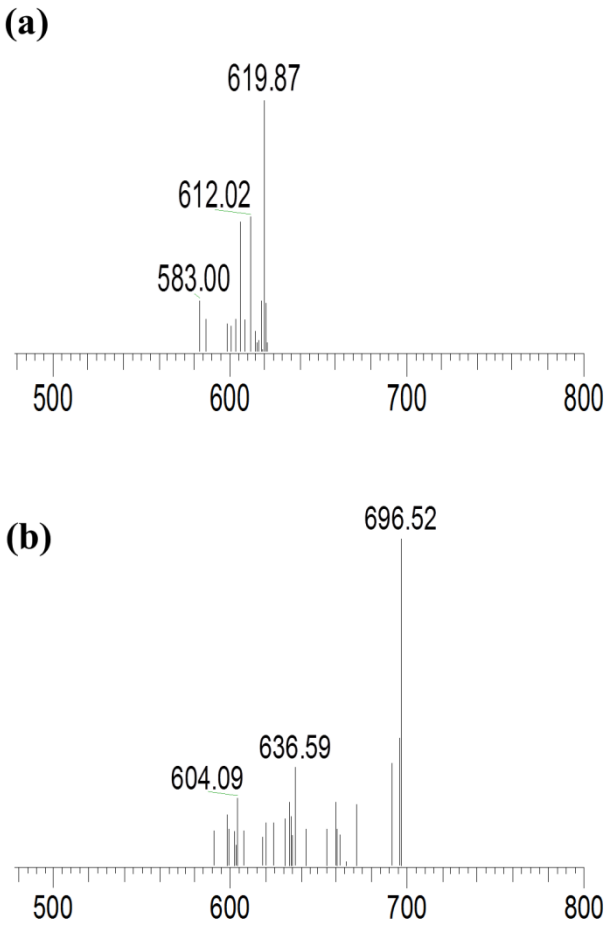

Fig. S22 MS spectra of the reaction products of **DTPAS** with Hg^{2+} (a) and Ag^{+} (b), the values are almost the same as the formula mass of **DTPAO** and **DTPAOS**, respectively.

Table S3 DTPAS detect Hg^{2+} and Ag^{+} in different actual water samples.

Water samples	Metal ions	Added (10^{-5} mol/L)	ICP-MS (10^{-5} mol/L)	Detected (10^{-5} mol/L)	Recovery (%)	RSD (%) (n=3)
Tap water	Hg^{2+}	3.0	2.95	2.91	97	0.67
	Ag^{+}	9.0	8.94	8.92	99	1.13
Lake water	Hg^{2+}	3.0	3.04	3.05	101	1.06
	Ag^{+}	9.0	9.08	8.87	98	1.64
Underground water	Hg^{2+}	3.0	2.98	3.13	104	0.89
	Ag^{+}	9.0	9.11	9.21	102	1.24

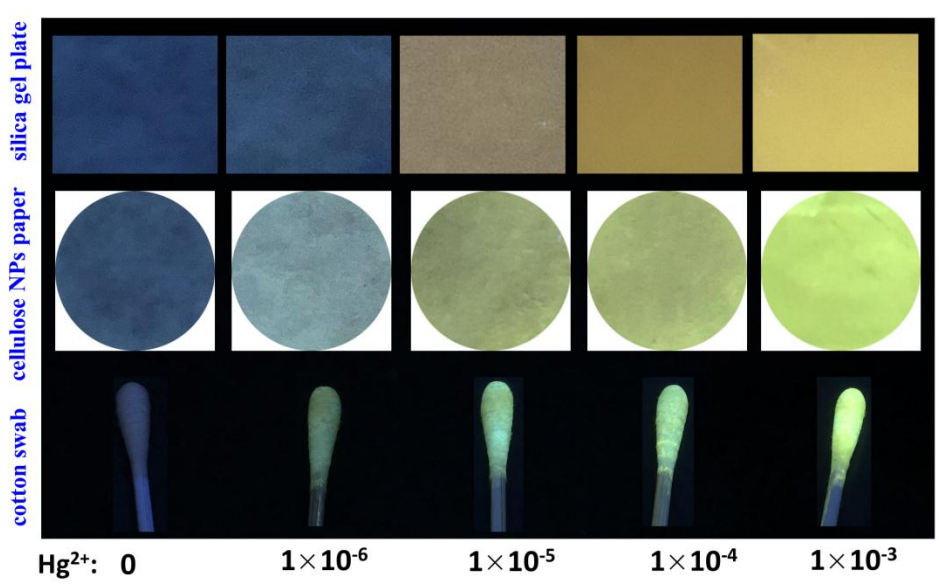

Fig. S23 Fluorescence responses of **DTPAS** encountered various Hg^{2+} contents in water with different solid mediums (silica gel plate, cellulose NPs paper and cotton swab).

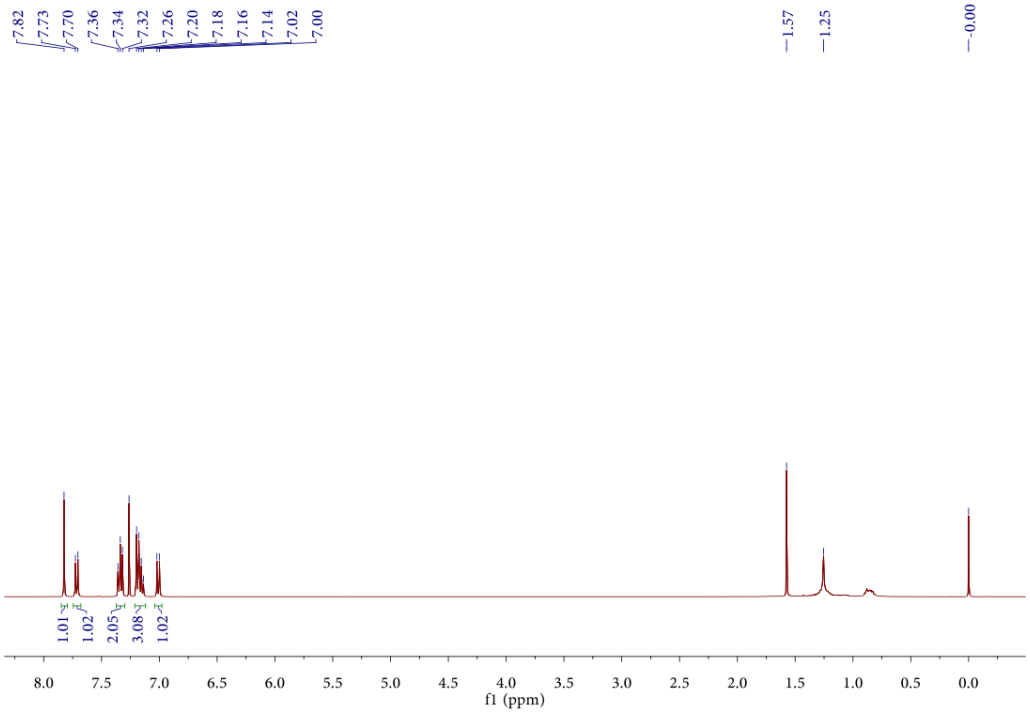

Fig. S24 ^{1}H NMR of **DTPAO** in $CDCl_3$.

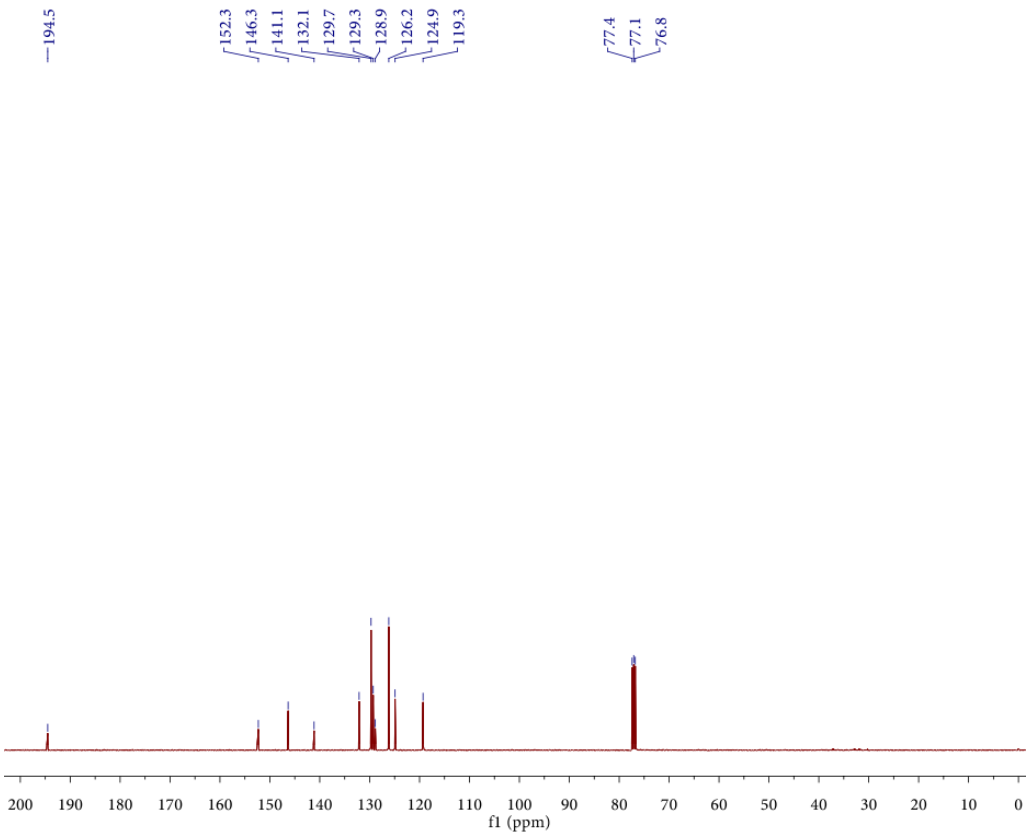

Fig. S25 ^{13}C NMR of **DTPAO** in $CDCl_3$.

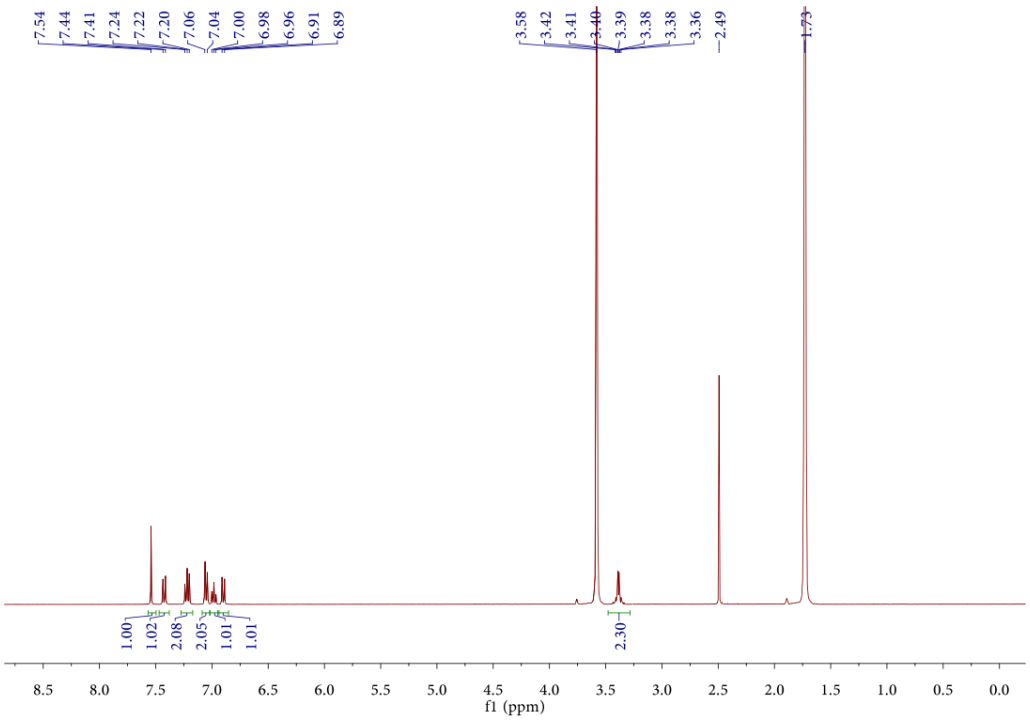

Fig. S26 ^{1}H NMR of **DTPAS** in THF-d_8.

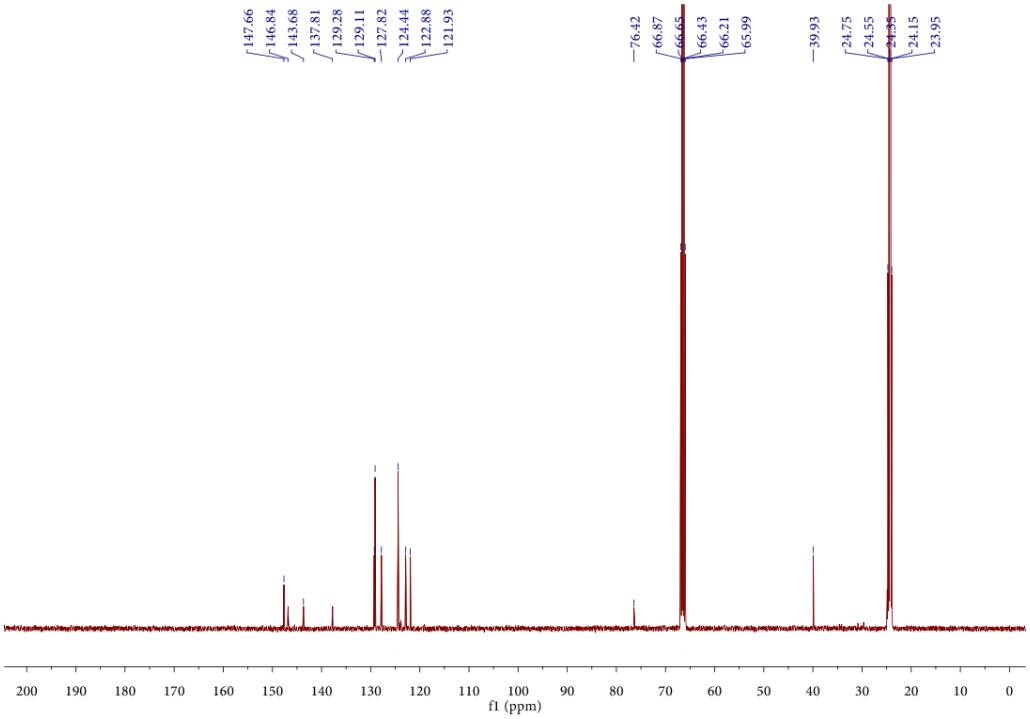

Fig. S27 ^{13}C NMR of **DTPAS** in THF-d_8.

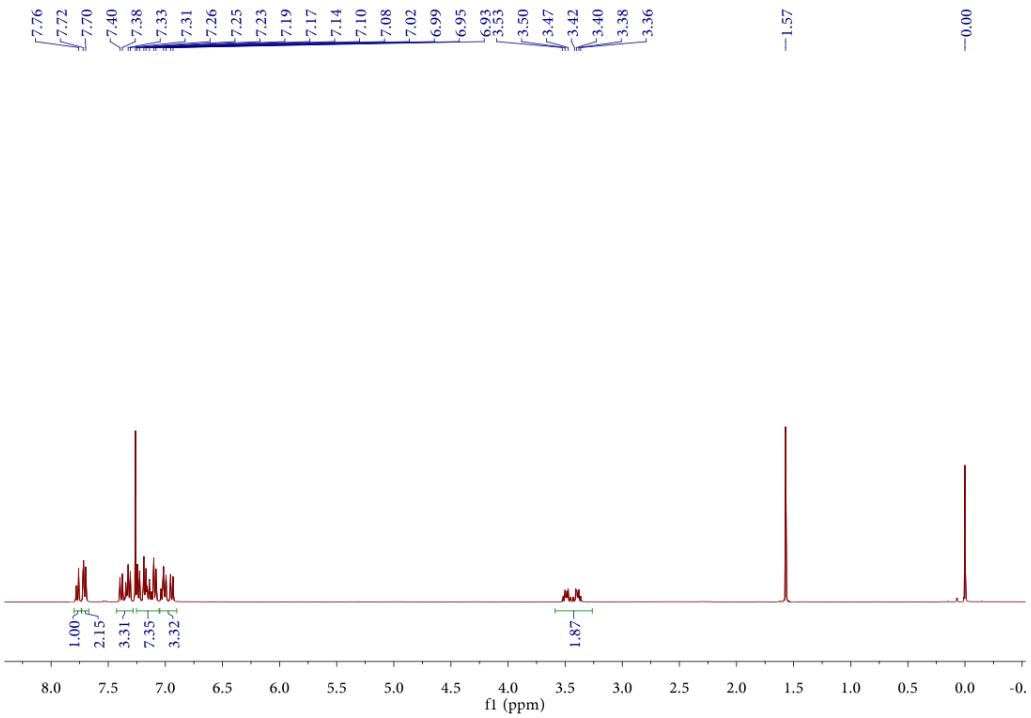

Fig. S28 ^{1}H NMR of **DTPAOS** in $CDCl_3$.

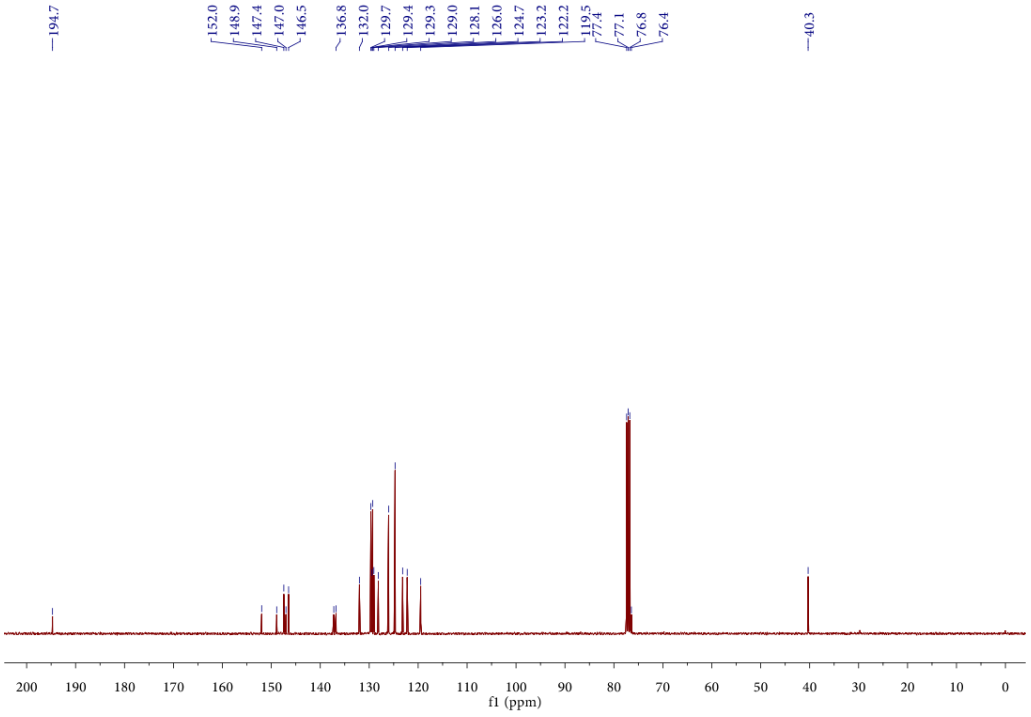

Fig. S29 ^{13}C NMR of **DTPAOS** in $CDCl_3$.